Journal of Power Sources 196 (2011) 9228–9237

Contents lists available at ScienceDirect

Journal of Power Sources

journal homepage: www.elsevier.com/locate/jpowsour

First-principles based microkinetic modeling of borohydride oxidation on a Au(1 1 1) electrode

Gholamreza Rostamikia[a], Alfonso J. Mendoza[b], Michael A. Hickner[b], Michael J. Janik[a,*]

[a] Department of Chemical Engineering, Pennsylvania State University, University Park, PA 16802, United States
[b] Department of Materials Science and Engineering, Pennsylvania State University, University Park, PA 16802, United States

ARTICLE INFO

Article history:
Received 26 May 2011
Received in revised form 11 July 2011
Accepted 12 July 2011
Available online 21 July 2011

Keywords:
Borohydride oxidation
DBFC
DFT
Electrocatalysis
Raman

ABSTRACT

Borohydride oxidation electrokinetics over the Au(1 1 1) surface are simulated using first-principles determined elementary rate constants and a microkinetic model. A method to approximate the potential dependent elementary step activation barriers based on density functional theory calculations is developed and applied to the minimum energy path for borohydride oxidation. Activation barriers of the equivalent non-electrochemical reactions are calculated and made potential dependent using the Butler–Volmer equation. The kinetic controlled region of the borohydride oxidation reaction linear sweep voltammogram over the Au(1 1 1) surface is simulated. The simulation results suggest that B–H bond containing species are stable surface intermediates at potentials where an oxidation current is observed. The predicted rate is most sensitive to the symmetry factor and the BH_2OH dissociation barrier. Surface-enhanced Raman spectroscopy confirms the presence of BH_3 as a stable intermediate.

1. Introduction

Increasing demand for mobile power conversion devices has motivated research directed towards developing a range of fuel cell technologies. Hydrogen fuel cells have attracted the most interest for large-scale applications like automobiles, however they are less interesting for small-scale power applications due to hydrogen storage and gas handling safety concerns. Alternatively, direct borohydride fuel cells (DBFCs) have the potential to convert chemical energy to electrical energy from a high energy density sodium borohydride aqueous fuel, making them attractive for small-scale, portable power applications. Poor anode efficiency limits DBFC application [1–4]. The mechanism of direct oxidation and competing hydrolysis reactions in alkaline media is unclear and difficult to study experimentally, therefore, kinetic modeling of the elementary reactions of borohydride oxidation can help to determine limiting steps and reactive intermediates to guide rational design of improved catalysts. We use density functional theory (DFT) studies combined with microkinetic modeling to predict the potential dependent rate of borohydride oxidation over the Au(1 1 1) electrode surface. Comparison between the simulated and experimental linear sweep voltammograms as well as Raman spectroscopy of adsorbed intermediates is used to corroborate the DFT-based reaction mechanism.

We previously studied the mechanism of borohydride oxidation and hydrolysis over gold and platinum surfaces using DFT methods [5,6]. We determined the preferred reaction path for borohydride oxidation over Au(1 1 1) and Pt(1 1 1) surfaces. We also identified the key energetic steps in direct oxidation and competing hydrolysis reactions. Our previous analysis utilized DFT-determined elementary reaction thermodynamics, however, reaction kinetics were not directly evaluated due to limitations in calculating potential dependent activation barriers with DFT. This motivates us to develop a simple method to calculate the potential dependent activation barriers for the borohydride oxidation reaction. Evaluation of activation barriers will help to clarify limiting elementary steps and determine energetic parameters which can be evaluated in designing a new catalyst with better activity and selectivity than gold and platinum electrodes. With approximate elementary step reaction barriers from DFT, potential dependent elementary rate constants are calculated and input to microkinetic models. Microkinetic models are then used to simulate electrokinetic experiments, such as linear sweep voltammetry, for comparison with experimental studies. DFT calculations and microkinetic modeling may then be coupled to predict the kinetics of yet untested catalyst formulations, providing a computational design tool.

For the complex $8e^-$ borohydride oxidation reaction, agreement between DFT-predicted and experimental voltammograms is not sufficient to verify the theoretically determined reaction mechanism. In this study, we used surface-enhanced Raman spectroscopy (SERS) [7] detection of stable species on roughened gold electrodes

* Corresponding author. Tel.: +1 814 863 9366; fax: +1 814 865 7846.
E-mail address: mjanik@psu.edu (M.J. Janik).

0378-7753/$ – see front matter © 2011 Elsevier B.V. All rights reserved.
doi:10.1016/j.jpowsour.2011.07.042

to further validate the DFT-predicted reaction mechanism. Gold is not an active catalyst for breaking B–H bonds and we use SERS to examine whether stable boron species with SERS-active B–H bonds are present at various electrode potentials.

In addition to the specific borohydride oxidation kinetics studied herein, a new method for determining potential dependent activation barriers from DFT calculations is presented. Atomistic modeling of elementary electrocatalytic rate constants is challenging, and few methods exist to compute potential dependent redox activation barriers from quantum mechanical methods. The reaction center model of Anderson has been applied to compute potential dependent barriers, however, it is restricted to an unrealistic representation of the electrode surface using a few metal atoms [7]. The double reference method developed by Filhol and Neurock [8,9] has been applied to non-redox elementary steps at the electrode surface [10], however, direct evaluation of barriers to electron transfer steps is restricted (currently applied in a single study [11]) due to the static nature of the electrolyte and limited unit cell size.

DFT evaluation of activation barriers for surface reactions not involving electron and ion transfer is well established. Herein, we present an approach to extrapolate potential dependent barriers for non-electrochemical hydrogenation/dehydrogenation reactions to their equivalent electrochemical redox reactions. Activation barriers for the non-electrochemical reaction are assigned to an appropriate equilibrium potential for the elementary reaction step. The barriers are then extrapolated utilizing the Butler–Volmer assumption that the activation barrier of a single redox reaction is linearly dependent on the potential with a symmetry factor β. For a single oxidation step:

$$E_a(V) = E_a^{\circ} - \beta(V - V_0) \quad (1)$$

where $E_a{}^{\circ}$ is activation barrier at the equilibrium potential V_0, and β is the symmetry factor. For most electrochemical systems the value of β is between 0.3 and 0.7 [12].

In this work, we predict the rate of borohydride electrooxidation on the Au(1 1 1) surface. Most of previous experimental studies have concluded that borohydride oxidation on the gold surface is a 7–8 electron process [13–15], however, some recent studies suggest that the oxidation might be a four electron process, also producing two hydrogen molecules at low potentials [16,17]. These studies did concur that the process at higher potentials is nearly a complete 8-electron process [16,17]. As a first approximation, we assume that borohydride oxidation on the gold surface is an 8-electron process, and any minor hydrogen production at lower potentials is neglected. Though Au electrodes are reasonably selective to the direct borohydride oxidation reaction, they suffer from large overpotentials due to slow oxidation kinetics. The limiting elementary reaction steps and stable surface intermediates are determined based on DFT and microkinetic modeling. A simulated linear sweep voltammogram (LSV) is reported and compared to the experimental LSV. SERS results confirm stable intermediates for the borohydride oxidation process over the Au electrode.

2. Research methods

2.1. Experimental methods

All chemicals were purchased from Sigma–Aldrich and used as received unless otherwise stated. Linear sweep voltammetry (LSV) was performed using a computer-controlled PARSTAT 2273 potentiostat (Princeton Applied Research). A three-electrode glass cell (125 mL, Pine Instruments) was outfitted with a 3 mm gold rotating disk working electrode (Metrohm) and a graphite rod (Sigma–Aldrich) counter electrode. The working electrode was polished to a mirror finish using 1 μm and 0.05 μm alumina paste (Pine Instruments). A single-junction Ag/AgCl (4 M KCl, Pine Instruments) reference electrode was employed and 2 M NaOH served as the electrolyte. A borohydride concentration of 0.03 M was used for LSV and SERS experiments. All the potentials reported here are converted to normal hydrogen electrode (NHE) scale.

For SERS experiments, the gold surface was roughened by cycling for 25 scans in a deoxygenated aqueous 0.1 M KCl solution between −0.08 V and 1.42 V with scan rate of 500 mV s^{-1} [18,19]. The electrode was then cleaned ultrasonically for 15 min in 18.5 MΩ water. A confocal Raman microscope (Renishaw inVia) with a 20 × 0.40 NA glass objective, 1200 lines cm^{-1} diffraction grating, a solid state 785 nm diode laser, and Pelletier cooled CCD detector was used to collect the SERS spectra.

The working electrode was placed in 0.03 M $NaBH_4$ and 2 M NaOH solution at a constant potential for 10 min. The electrode was rotated at 500 rpm to avoid accumulation of hydrogen gas on the surface. After the 10 min potential hold, the electrode was removed from solution under potential and the SERS was collected immediately from the surface of the electrode. Co-additions of 5 scans (1950–2250 cm^{-1}) with an exposure of 10 s were used to increase the signal to noise ratios of the spectra.

2.2. Computational methods

Density functional theory calculations were performed using the ab initio total energy and molecular-dynamics Vienna ab initio simulation program (VASP) developed at the Institute for Material Physics at the University of Vienna [20–22]. To represent the electronic structure, the projector augmented wave method [23,24] was used with a plane wave basis set (cut-off energy 400 eV) and the Perdew–Wang [25] form of the generalized gradient approximation. To optimize the structures, a 3 * 3 * 1 Monkhorst–Pack grid was used followed by a single-point calculation using a 4 * 4 * 1 grid. To optimize the structures, forces on all atoms were minimized to values lower than 0.05 eV $Å^{-1}$. The climbing image nudged elastic band method (CI-NEB) was used to isolate the transition states of elementary reactions on the surface [26,27]. Four images with equal spacing were used between the initial and final state. The transition state was identified as the image with the highest energy whereas the tangent force is less than 0.04 eV $Å^{-1}$. Transition states were confirmed to have a single imaginary vibrational frequency.

Similar to our previous studies on borohydride oxidation on Au(1 1 1) [5] and Pt(1 1 1) [6] surfaces, we used a vacuum-slab model of the surface. Ion adsorption and surface reaction energies as well as optimized adsorbate structures were previously reported [5]. Our initial study of borohydride oxidation on Au(1 1 1) neglected the possible formation of a $B(OH)_4{}^-$ product or reaction through a $B(OH)_3{}^*$ surface intermediate (where "*" is used throughout to note surface bound species). The binding energy (BE) of $B(OH)_3{}^*$ was calculated using the following equation:

$$B(OH)_3 + * \rightarrow B(OH)_3{}^*$$

$$BE = E_{DFT,B(OH)_3^*} - E_* - E_{DFT,B(OH)_3} \quad (2)$$

where $E_{DFT,B(OH)_3^*}$ is the energy of adsorbed species, E_* is the energy of bare surface and $E_{DFT,B(OH)_3}$ is the energy of isolated $B(OH)_3$ species.

2.2.1. Calculation of potential dependent adsorption equilibrium constants

The adsorption of $BH_4{}^-$ ions on the surface was considered to be at equilibrium with the bulk solution at all potentials of interest:

$$BH_4{}^-{}_{(aq)} + H_2O^* \leftrightarrow BH_4{}^* + H_2O_{(aq)} + e^-$$

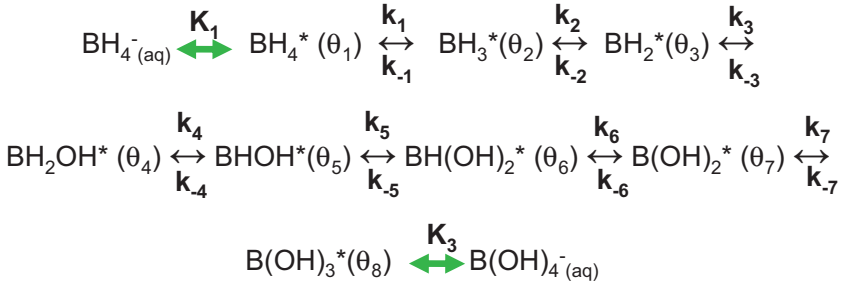

Fig. 1. Minimum energy path for borohydride oxidation over Au(1 1 1) surface. Each reaction step produces an electron (other than the final product desorption step) and consumes a OH^- species either to form an H_2O molecule or a B–OH bond.

For the BH_4^- concentration of 0.03 M, the adsorption of BH_4^-, with one molecule over nine Au(1 1 1) surface atoms is favorable (Gibb's free energy change exergonic) at potentials greater than $0.05V_{NHE}$, as determined in our previous work [5]. The Gibbs free energy change of borohydride adsorption (ΔG_1), relative to the 0.03 M aqueous concentration, is therefore expressed as:

$$\Delta G_1 = (0.05 - V_{NHE})e^- \tag{3}$$

where e^- represents the electron charge and is equal to 1 when using an energy unit of eV. The equilibrium constant for this adsorption step (K_1) is then

$$K_1 = \exp\left(\frac{-\Delta G_1}{RT}\right) = \frac{\theta_{BH_4^*}}{\theta_{H_2O^*}[BH_4^-]} \tag{4}$$

where $\theta_{BH_4^*}$ is the surface fraction covered with BH_4^* species and $\theta_{H_2O^*}$ is the surface coverage of water (replacing the typical free surface coverage due to the aqueous environment). The concentration of the borohydride anion is included in the denominator, though rigorously this should be noted as the species activity. This assumes an activity coefficient of 1, and the concentration in the denominator is non-dimensionalized by the 0.03 M concentration used in calculation of ΔG_1.

The equilibrium constant for the BH_4^- ion adsorption is therefore potential dependent, and we approximate that the adsorption free energy is coverage independent.

Similarly, for the adsorption of OH^- species ($[OH^-] = 2$ M, calculated for one OH group per 9 surface atoms) the equilibrium constant is [5]:

$$K_2 = \exp\left(\frac{-\Delta G_2}{RT}\right) = \frac{\theta_{OH^*}}{\theta_{H_2O^*}[OH^-]} \tag{5}$$

where

$$\Delta G_2 = (0.29 - V_{NHE})e^- \tag{6}$$

The dimensionless hydroxyl concentration, non-dimensionalized by the reference concentration of 2 M, is included in the denominator of Eq. (5) rather than the more rigorous activity expression.

2.2.2. Calculation of the desorption equilibrium constant of boric acid

We have previously concluded that boric acid is the final product of the surface borohydride oxidation reaction over the Au(1 1 1) electrode [6]. The product boric acid may then reaction in the solution phase to produce the hydrated borate anion:

$$B(OH)_{3(aq)} + OH^-{}_{(aq)} \leftrightarrow B(OH)_4{}^-{}_{(aq)} \tag{7}$$

The surface adsorbed boric acid species, $B(OH)_3{}^*$, is assumed to be in equilibrium with the $B(OH)_4{}^-$ ion in the solution phase. The free energy of desorption of $B(OH)_3{}^*$ may be calculated by evaluating the free energy change of replacing adsorbed $B(OH)_3{}^*$ with H_2O followed by the equilibrium of Eq. (7):

$$\Delta G_3 = G_{H_2O*} + G_{B(OH)_4^-} - G_{OH_{aq}^-} - G_{H_2O_{aq}} - G_{B(OH)_3^*} \tag{8}$$

The calculated value of ΔG_3 is −0.74 eV.

The evaluation of the free energy of the solvated and surface bound species is discussed in our previous publications [5,6].

The equilibrium constant for the $B(OH)_3{}^*$ desorption step is then:

$$K_3 = \exp\left(\frac{-\Delta G_3}{RT}\right) = \frac{\theta_{H_2O^*}[B(OH)_4^-]}{\theta_{B(OH)_3{}^*}[OH^-]} \tag{9}$$

2.2.3. Potential dependent activation barriers

Density functional theory calculations do not trivially provide potential dependent activation barriers for redox reactions. We calculated non-potential dependent activation barriers for the equivalent chemical reactions on the Au(1 1 1) surface, and extrapolated these to be potential dependent using a Butler–Volmer formalism. The overall oxidation reaction is presumed to proceed through the minimum energy path, and competing less favorable elementary steps are not considered.

The elementary oxidation steps on the Au(1 1 1) surface could be categorized to three different types of reaction: (1) B–H cleavage reactions, (2) B–O bond formation reactions and (3) O–H bond cleavage reactions. Breaking O–H bonds is not favorable as gold is a poor catalyst for activating these bonds, and we conclude that the final eight electron oxidation product of the surface reaction is boric acid, $B(OH)_3$. Alternatively, B–O formation reactions are very favorable and exothermic on the gold surface and our DFT calculations indicate that the activation barriers of these reactions are negligible. Activating B–H bonds on the surface limits the overall oxidation process.

Fig. 1 shows the minimum energy path for borohydride oxidation on the Au(1 1 1) surface. In Fig. 1, k_x represents the rate constant for each elementary electrooxidation reaction and k_{-x} represents the reverse reduction rate constant. The OH^-, H_2O, and electron species involved in each reaction step are left off of Fig. 1 for simplicity. Each reaction step, other than the final desorption step, produces an electron. All reaction steps, other than the initial BH_4^- adsorption, consume a OH^- species to either form a water molecule or a B–OH bond.

For a typical B–H breaking step on the surface, the non-electrochemical dehydrogenation elementary reaction can be written as:

$$A\text{–}H^* \rightarrow A^* + H^* \tag{10}$$

The equivalent electro-oxidation step for this reaction is:

$$A\text{–}H^* + OH^-{}_{aq} \rightarrow A^* + H_2O_{aq} + e^- \tag{11}$$

For the electrocatalytic reaction, the B–H bond is activated through interaction with the catalyst surface. We approximate that the

activation barriers of these two reactions are equivalent at the electrochemical potential at which the chemical potential of the H^* product is in equilibrium with its desorbed product:

$$H^* + OH^-{}_{aq} \rightarrow H_2O_{aq} + e^- + * \quad (12)$$

With this assumption, the activation barrier for the non-electrochemical dehydrogenation reaction is assigned to the potential at which the surface H^* species has the same chemical potential as the redox reaction product. At this potential, the dissociated hydrogen atom has equal thermodynamic preference to adsorb to the surface or oxidize to produce a proton and an electron.

The activation barriers for the non-electrochemical reaction 10 are calculated with the vacuum-slab DFT model. Then, similar to the Butler–Volmer expression, potential dependent activation barriers for oxidation reactions are linearly related to the equivalent electrochemical reaction activation barriers using a symmetry factor. For example, the activation barrier of oxidative dissociation of BH_4^* ($E_a(V)$), $BH_4^* + OH^-{}_{(aq)} \rightarrow BH_3^* + H_2O_{(aq)} + e$ is written as:

$$E_{a_1}(V) = E_{a_1}{}^\circ - \beta\,(V - V_0) \quad (13)$$

where $E_{a_1}{}^\circ$ is the activation barrier for the chemical step, β is the symmetry factor, and V_0 is the equilibrium potential for the oxidation of surface hydrogen.

2.2.4. Calculation of potential dependent rate constants

Using transition state theory, an Arrhenius form is considered for the elementary rate constants. For example, for the initial B–H dissociation step:

$$k_1 = A_1 * e^{-Ea_1(V)/RT} \quad (14)$$

The pre-exponential factor is approximated as:

$$A_1 = \frac{\tau k_b T}{h} \quad (15)$$

where k_b is the Boltzman constant, T is the absolute temperature, h is Planck's constant, and τ represents the probability that the system will go over the barrier. A reasonable value of $\tau = 0.5$ is used in all calculations. The rate of any surface reaction is calculated as:

$$-r_n = k_n \theta_n \quad (16)$$

where r_n represents the rate of nth reaction, k_n is the rate constant for the nth step, and θ_n is the surface fraction of the species being converted in step n. The units of the rate calculated are s^{-1} $site^{-1}$. Since each elementary reaction produces 1 electron, the current will be in units of electrons s^{-1} $site^{-1}$.

2.2.5. Micro-kinetic model construction

A set of algebraic and differential equations are written as:

$$\frac{d\theta_2}{dt} = k_1\theta_1 - k_2\theta_2 + k_{-2}\theta_3 - k_{-1}\theta_2 \quad (17)$$

$$\frac{d\theta_3}{dt} = k_2\theta_2 - k_3\theta_3 - k_{-2}\theta_3 + k_{-3}\theta_4 \quad (18)$$

$$\frac{d\theta_4}{dt} = k_3\theta_3 - k_4\theta_4 - k_{-3}\theta_4 + k_{-4}\theta_5 \quad (19)$$

$$\frac{d\theta_5}{dt} = k_4\theta_4 - k_5\theta_5 - k_{-4}\theta_5 + k_{-5}\theta_6 \quad (20)$$

$$\frac{d\theta_6}{dt} = k_5\theta_5 - k_6\theta_6 - k_{-5}\theta_6 + k_{-6}\theta_7 \quad (21)$$

$$\frac{d\theta_7}{dt} = k_6\theta_6 - k_7\theta_7 - k_{-6}\theta_7 + k_{-7}\theta_8 \quad (22)$$

$$\sum \theta = 1 \quad (23)$$

$$\theta_1 = \frac{K_1\theta_{10}}{[BH_4^-]} \quad (24)$$

$$\theta_9 = \frac{K_2\,\theta_{10}}{[OH^-]} \quad (25)$$

where θ_1 to θ_8 were introduced in Fig. 1 and correspond to the surface fraction of different boron containing intermediate species. θ_9 is the surface fraction of OH species and θ_{10} is the "empty" surface fraction, or better written in solution as the fraction of surface which is covered with water. Since the concentration of $B(OH)_4^-$ ions is very small, 1×10^{-6} M is assigned for the $B(OH)_4^-$ concentration, and this is used to evaluate the $B(OH)_3{}^*$ surface concentration as described above. The value of 1×10^{-6} M represents an approximate concentration value for the $B(OH)_4^-$ ion given mass transfer into the stagnant solution from the surface region [28]. Though this value is relatively arbitrary, the exact value has little impact on the simulated kinetics as product adsorption is negligible and the reverse reduction reaction rates are miniscule at the high oxidation overpotentials necessary to observe an anodic current.

In the set of differential equations, all rate constants and equilibrium constants are dependent on the electrode potential. The electrode potential can then be made time dependent given an initial potential and sweep rate in the LSV experiment. The set of algebraic and differential equations can be solved simultaneously to find the time/potential dependent current of borohydride oxidation over the Au(1 1 1) surface. Numerical solution requires a small time step to reach reasonable real times because both extremely fast and slow reactions are included in the model. As a first approximation, we assume that the surface reactions reach a quasi-steady state as the potential is varied. Because the time derivative of surface intermediates is approximated as zero, $d\theta_n/dt$ is equal to zero. This leaves a set of algebraic equations which can be solved at each potential. The potential dependent fractional coverages of all species (θ_n) are determined and used to calculate the reaction rate, as described in the next section.

2.2.6. Calculating the current from the microkinetic model

As the overall oxidation process produces eight electrons, the overall current could be calculated by multiplying the rate of any surface oxidation reaction by eight. For example:

$$i_c = 8k_7q_7 \quad \text{in units of electrons } s^{-1} \quad \text{surface site}^{-1}$$

To convert the per site current to a per area current, we multiply by the electronic charge and the number of surface sites per area. The electrode used experimentally has a surface area (A) of 7.065×10^{-2} cm^2. For the Au(1 1 1) surface, the area occupied by one atom (a) is 7.0298×10^{-16} cm^2. The number of atoms on the electrode surface is:

$$N = \frac{A}{a} \quad (26)$$

If we assume that n atoms make one reaction site on the surface, then the number of active sites (S) is:

$$S = \frac{N}{n} \quad (27)$$

A value of $n = 3$ is assigned for number of surface atoms per active site. This value is based on the size of intermediates, as all surface intermediates are similar in size to three Au surface atoms. The effect of changing n is discussed in the results section.

The computationally calculated current (I) is given by:

$$I = 8eSk_7\theta_7\left(\frac{A}{s}\right) \quad (28)$$

where e is the electronic charge.

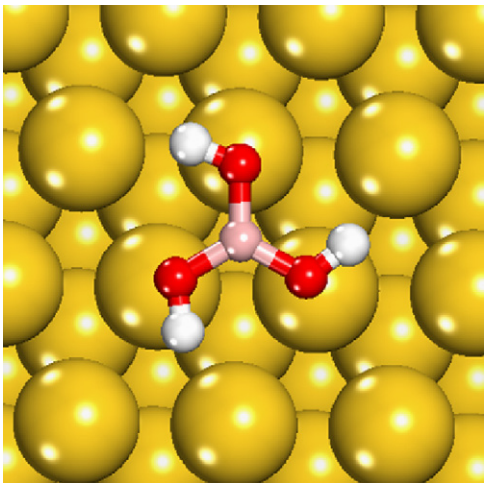

Fig. 2. Adsorption configuration of $B(OH)_3$ on the Au(1 1 1) surface.

3. Results and discussion

The electro-oxidation of borohydride is modeled over the Au(1 1 1) surface. As our previous paper applying DFT to the study of borohydride oxidation over the Au(1 1 1) surface neglected the possibility of forming boric acid the final $8e^-$ product, the preferred binding site of boric acid is first reported in Section 3.1. The activation barriers for the favorable oxidation path are presented in Section 3.2. The simulated borohydride oxidation LSV results are presented in Section 3.6 and compared with experiment. Raman spectroscopy results are presented in Section 3.7 for further corroboration of the computationally predicted reaction mechanism.

3.1. Preferred binding site of boric acid on the Au(1 1 1) surface

The binding energy and optimal binding configuration of borohydride oxidation intermediates was previously reported [5]. This study did not consider production of a final boric acid $(B(OH)_3)^*$ product, which has since been determined as favored over BO_2^* as the final product of the surface oxidation reaction. Fig. 2 illustrates the most stable adsorption configuration for $B(OH)_3{}^*$ on the Au(1 1 1) surface. $B(OH)_3{}^*$ species are stable molecules and have a weak interaction with the Au(1 1 1) surface. The binding energy of these species to the Au(1 1 1) surface is −0.3 eV. The desorption of these species in aqueous media therefore has only a slight activation barrier and will likely be mass transfer limited.

3.2. Non-electrochemical activation barriers for the preferred reaction path

The activation barrier for the initial dehydrogenation reaction was previously reported [5]:

$$BH_4^* \rightarrow BH_3^* + H^* \quad E_{act} = 0.37 \text{ eV } (36 \text{ kJ mol}^{-1}) \tag{29}$$

The activation barriers for the B–O formation reactions

$$BH_2{}^* + OH^* \rightarrow BH_2OH^*$$

$$BHOH^* + OH^* \rightarrow BH(OH)_2{}^*$$

$$B(OH)_2{}^* + OH^* \rightarrow B(OH)_3{}^*$$

were evaluated and all found to be extremely small (≤0.01 eV). For microkinetic modeling, a barrier of 0.01 eV is assigned for all B–O formation steps.

The transition state for $BH_3{}^*$ dehydrogenation to $BH_2{}^*$ and H^* is illustrated in Fig. 3. The barrier for this reaction is 0.81 eV (78 kJ mol^{-1}). The dissociating B–H bond stretches from 1.23 Å in the $BH_3{}^*$ state to 2.3 Å at the transition state. A single imaginary vibrational frequency of $i284$ cm^{-1} confirms that the state in Fig. 3b is a transition state.

The equilibrium and transition states for BH_2OH^* dehydrogenation to $BHOH^*$ and H^* are illustrated in Fig. 4. This step has the highest activation barrier among the B–H dissociation steps. The activation barrier is 1.06 eV (102 kJ mol^{-1}). The B–H bond extends from 1.2 Å at the initial state to 1.9 Å at the transition state. An imaginary vibrational frequency of $i406$ cm^{-1} confirms that Fig. 4b represents a transition state.

The transition state for $BH(OH)_2{}^*$ dissociation to $B(OH)_2{}^*$ and H^* is illustrated in Fig. 5. Similar to BH_2OH^* dissociation, this step has a high barrier (0.91 eV or 88 kJ mol^{-1}). The dissociating bond extends from 1.2 Å at the initial state to 2.3 Å at the transition state. An imaginary vibrational frequency of $i282$ cm^{-1} confirms the transition state.

Table 1 lists the activation barriers for B–H dehydrogenation and B–O formation reactions on the Au(1 1 1) surface.

3.3. Surface hydrogen oxidation potential on the Au(1 1 1) surface

The activation barriers calculated for dehydrogenation reactions are assigned to a specific potential by approximating that they represent the appropriate barrier at the chemical potential for which the product H^* species is in equilibrium with solution, as expressed in Eq. (12). Assuming that Eq. (12) is at equilibrium, for a 1/9 monolayer of hydrogen atoms on the surface and pH of 14.26, the

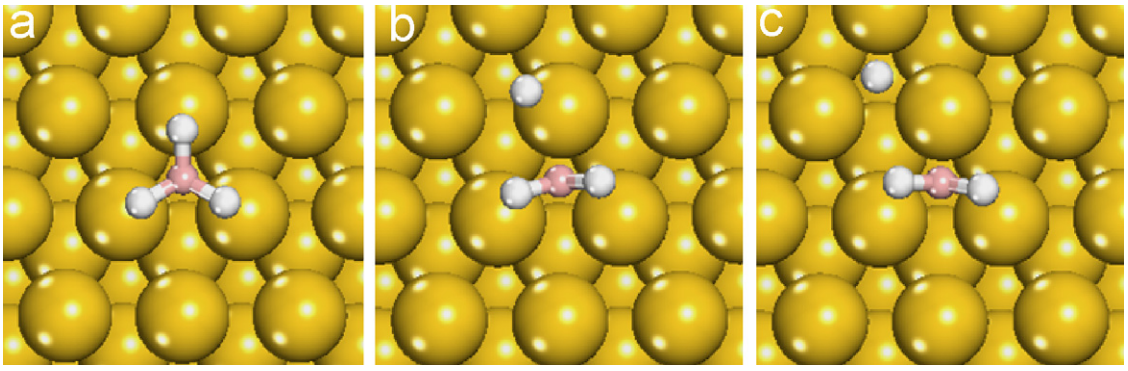

Fig. 3. $BH_3{}^*$ dehydrogenation to $BH_2{}^*$ and H^* over the Au(1 1 1) surface: (a) initial state, (b) transition state, and (c) final state.

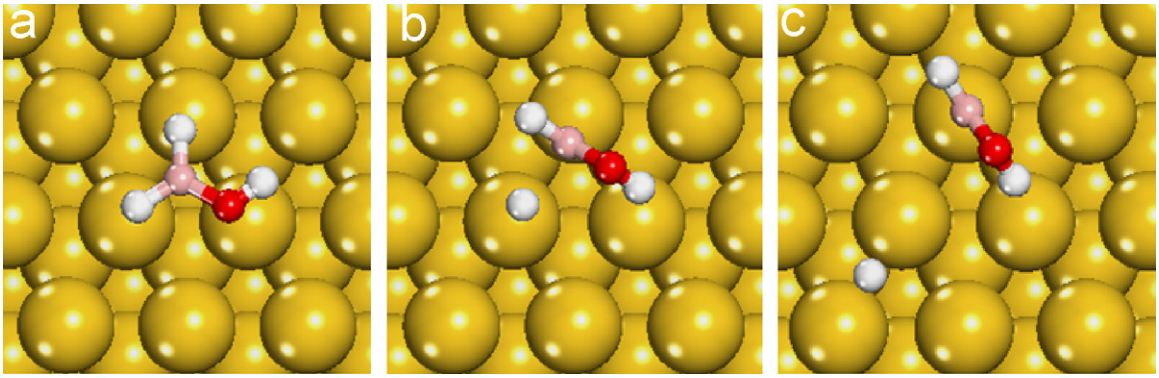

Fig. 4. Dehydrogenation of BH_2OH^* to BHOH* and H* over the Au(1 1 1) surface: (a) initial state, (b) transition state, and (c) final state.

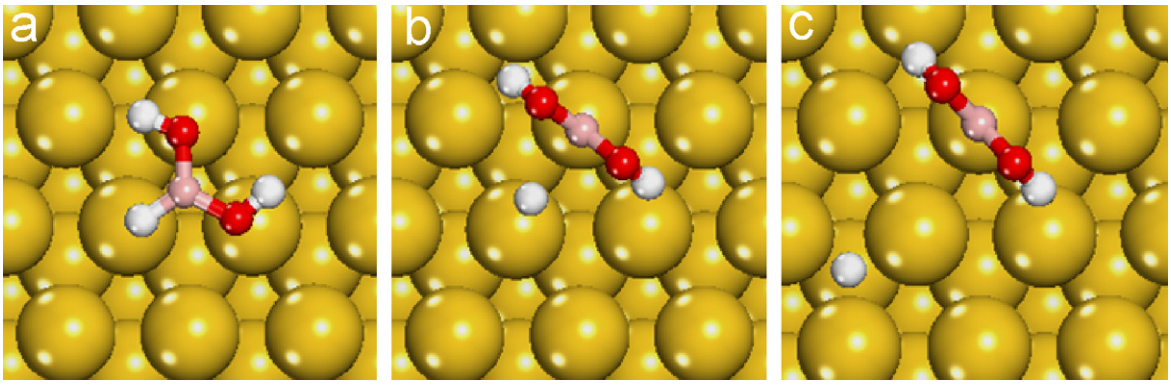

Fig. 5. Dehydrogenation of $BH(OH)_2^*$ to $B(OH)_2$* and H* over the Au(1 1 1) surface: (a) initial state, (b) transition state, and (c) final state.

equilibrium potential for surface hydrogen oxidation is calculated via:

$$V_0(NHE) = G_{H_2O_{aq}} + G_* - G_{H^*} - G_{OH^-_{aq}} - 4.6 \quad (30)$$

where 4.6 is conversion factor between absolute (vacuum scale) potential and the normal hydrogen electrode scale [5] determined using DFT methods consistent with those used herein. The value of V_0 calculated using Eq. (30) is −1.19 V.

3.4. Potential dependent rate constants for elementary oxidation reactions

Given the non-electrochemical barriers in Table 1 and the calculated equilibrium potential for the H* desorption, potential dependent rate constants for elementary reactions are calculated via Eq. (14). The potential dependent activation barriers for all steps are calculated using Eq. (13), with V_0 equal to $-1.19V(NHE)$ and E_a° from Table 1. Table 2 gives the potential dependent activation barriers for all elementary forward reaction steps of the minimum energy path.

For the backward (reduction) reactions the potential dependent activation barriers is calculated similarly. For example:

$$Ea_{1b}(V) = Ea^\circ_{1b} + \alpha(V + 1.19)$$

where $\alpha = 1 - \beta$ is the symmetry factor of the backward reaction [12].

The pre-exponential factor for the rate constants is calculated via Eq. (15). At room temperature (298 K), the calculated pre-exponential factor is $3.1 \times 10^{12}\ s^{-1}\ site^{-1}$. An average value of τ equal to 0.5 is used within the pre-exponential factor.

Fig. 6 presents the elementary reaction energetics and activation barriers of elementary reactions for the preferred oxidation path at −0.2 V and −1 V. A value of $\beta = 0.44$ is considered for symmetry factor and is discussed in Section 3.6. Fig. 6 shows that at −1 V, initial BH_4^- adsorption is not favorable and B–H bond dissociation steps present high barriers. At −0.2 V, all barriers become accessible at room temperature and the overall oxidation reaction will proceed.

Table 1
Activation barriers (eV) for elementary B–H dissociation and B–O formation reactions and the backward reactions over the Au(1 1 1) surface.

Reaction	E_a forward reaction	E_a backward reaction
(1) $BH_4^* \leftrightarrow BH_3^* + H^*$	$E_{a\,1f} = 0.37$	$E_{a\,1b} = 0.16$
(2) $BH_3^* \leftrightarrow BH_2^* + H^*$	$E_{a\,2f} = 0.81$	$E_{a\,2b} = 0.48$
(3) $BH_2^* + OH^* \leftrightarrow BH_2OH^*$	$E_{a\,3f}$ = Negligible (<0.01)	$E_{a\,3b} = 2.63$
(4) $BH_2OH^* \leftrightarrow BHOH^* + H^*$	$E_{a\,4f} = 1.06$	$E_{a\,4b} = 0.67$
(5) $BHOH^* + OH^* \leftrightarrow BH(OH)_2^*$	$E_{a\,5f}$ = Negligible	$E_{a\,5b} = 2.60$
(6) $BH(OH)_2^* \leftrightarrow B(OH)_2^* + H^*$	$E_{a\,6f} = 0.91$	$E_{a\,6b} = 0.78$
(7) $B(OH)_2^* + OH^* \leftrightarrow B(OH)_3^*$	$E_{a\,7f}$ = Negligible	$E_{a\,7b} = 2.72$

Table 2
Potential dependent activation barriers (eV) for elementary oxidation reactions of borohydride over the Au(1 1 1) surface.

Reactions	E_a (V)
(1) $BH_4^* + OH^- \leftrightarrow BH_3^* + H_2O + e^-$	$E_{a\,1f} = 0.37 - \beta\,(V + 1.19)$
(2) $BH_3^* + OH^- \leftrightarrow BH_2^* + H_2O + e^-$	$E_{a\,2f} = 0.81 - \beta\,(V + 1.19)$
(3) $BH_3^* + OH^- \leftrightarrow BH_2OH^* + e^-$	$E_{a\,3f}$ = Negligible (<0.01)
(4) $BH_2OH^* + OH^- \leftrightarrow BHOH^* + H_2O + e^-$	$E_{a\,4f} = 1.06 - \beta\,(V + 1.19)$
(5) $BHOH^* + OH^- \leftrightarrow BH(OH)_2^* + e^-$	$E_{a\,5f}$ = Negligible
(6) $BH(OH)_2^* + OH^- \leftrightarrow B(OH)_2^* + H_2O + e^-$	$E_{a\,6f} = 0.91 - \beta\,(V + 1.19)$
(7) $B(OH)^* + OH^- \leftrightarrow B(OH)_3^* + e^-$	$E_{a\,7f}$ = Negligible

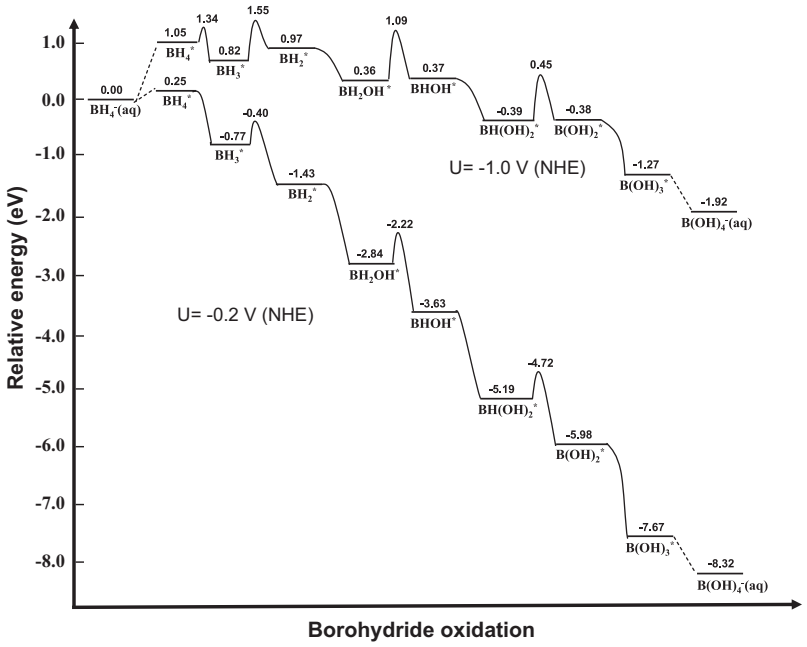

Fig. 6. Reaction energetics and activation barriers of the borohydride oxidation preferred path at two different potentials, $\beta = 0.44$, $[BH_4^-] = 0.03$ M, $[OH^-] = 2$ M, $T = 298$.

3.5. Experimental linear sweep voltammetry

Linear sweep voltammetry data for borohydride oxidation is presented in Fig. 7 for different scan rates (5, 10 and 25 mV s^{-1}). At potentials higher than −0.35 V, the reaction rate is affected by mass transfer and the current varies with scan rate. At potentials lower than −0.35 V, mass transfer has minimal effect on the current, the current is nearly independent of scan rate, and the oxidation process is controlled by kinetic limitations. Similar currents for different scan rates also suggest that the surface reactions reach a quasi-steady state at each potential as the potential is scanned. Therefore, at potentials lower than −0.35 V, we may approximate that the current is not time dependent and only depends on potential.

3.6. Simulated linear sweep voltammogram

Eqs. (19)–(25) were solved at each potential to determine the simulated current as a function of potential. Different values of symmetry factor were considered. Based on experimental LSV results, the simulated current was limited to values lower than 400 μA to avoid consideration of transport limitations in the system. Fig. 8 compares the experimental LSV data and simulation results for three different symmetry factor values. A single symmetry factor was used for all reaction steps; the evaluation of symmetry factors directly from DFT calculations will be a subject of future study. Data in Fig. 8 assumes 3 surface atoms as one active site.

For β values of 0.5, the simulation overestimates the oxidation current. The value of 0.5 is a reasonable approximate value

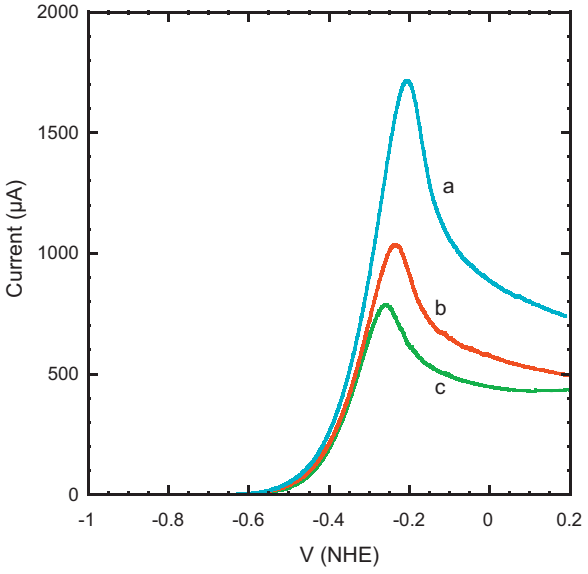

Fig. 7. Linear sweep voltammogram of borohydride oxidation over a gold electrode, $[BH_4^-] = 0.03$ M, $[OH^-] = 2$ M, $T = 298$ K, electrode diameter = 3 mm, scan rates: (a) 25 mV s^{-1}, (b) 10 mV s^{-1}, and (c) 5 mV s^{-1}.

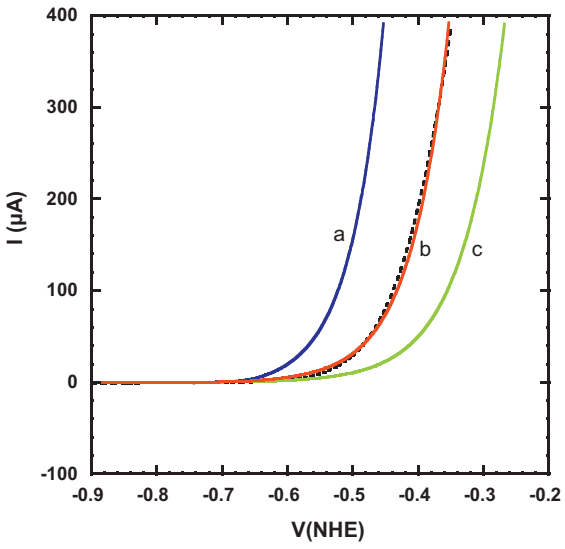

Fig. 8. Simulated (solid) and experimental (dashed) linear sweep voltammograms of borohydride over the gold electrode. Different values of symmetry factor are considered, $[BH_4^-] = 0.03$ M, $[OH^-] = 2$ M, $T = 298$ K, disk diameter = 3 mm, scan rate = 5 mV s^{-1}: (a) $\beta = 0.5$, (b) $\beta = 0.44$, (c) $\beta = 0.4$.

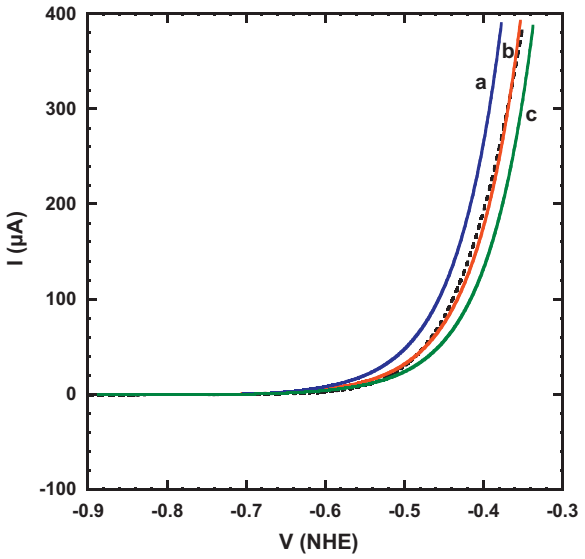

Fig. 9. Computational (solid) and experimental (dashed) data for linear sweep voltammetry of borohydride over the gold electrode. Effect of assuming different values of surface atoms per surface site in the model is presented, $[BH_4^-] = 0.03$ M, $[OH^-] = 2$ M, $T = 298$ K, disk diameter = 3 mm, scan rate = 5 mV s^{-1}: (a) $n = 2$, (b) $n = 3$, (c) $n = 4$.

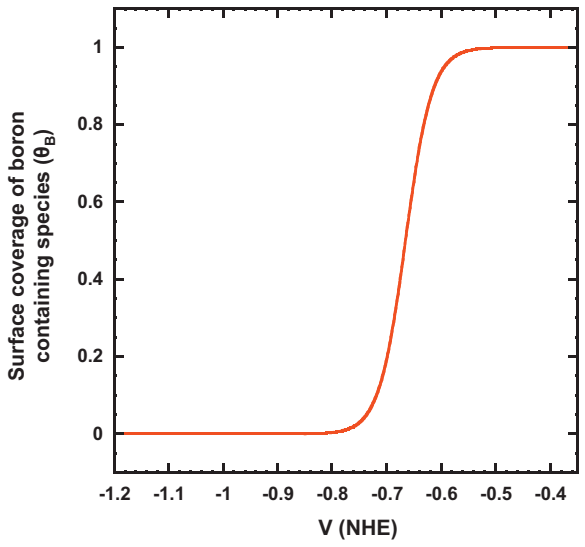

Fig. 10. Surface coverage of boron containing intermediate on the Au(1 1 1) surface as a function of potential from the kinetic model; $n = 3$, $\beta = 0.44$.

in absence of actual data, however, typical β values fall between 0.3 and 0.7 [12]. For β equal to 0.44, experimental and simulation results are in agreement. Clearly, the take-off potential and oxidation current are highly sensitive to the β value, and the need to approximate this value is a limitation of the methods used. Deviations from 0.5 can be approximated by considering the variable interactions of the equilibrium and transition state dipole moments with the interfacial electric field, and this will be a subject for future studies.

Fig. 9 presents the effect on n (number of surface atoms per surface site) on the computational current calculated from the kinetic model. Based on the size of the reaction intermediate molecules we initially considered a reasonable value of n equal to 3 in our calculation. Choosing different n values changes the absolute magnitude of the I–V curve. For a value of n equal to 2, the I–V curve shifts to lower potentials due to a higher number of surface sites per physical area. A value of n equal to 2 is likely not reasonable due to the size of the intermediates molecules. Increasing n to 4 decreases the current at a given potential. The effect of the n value on the computational current is lower than the effect of symmetry factor β, as reasonable n values are not beyond the 2–4 range.

Fig. 10 shows the surface coverage of boron containing intermediates (θ_B summed over all intermediates) on the Au(1 1 1) surface as a function of electrode potential. The modeling results suggest that BH_2OH^* is the most abundant surface intermediate and the Au(1 1 1) surface will be nearly completely covered by this species at potentials for which the oxidation current is substantial. At the potential of −0.55 V, the surface fractional coverage of BH_2OH exceeds 0.99 indicating essentially a full monolayer (1 BH_2OH species per 3 Au surface atoms). At potentials higher than −0.55 V the oxidation reaction is limited by the oxidation rate of this species. This is a direct consequence of the BH_2OH oxidation reaction barrier being larger than for all other elementary steps.

The predicted rate of reaction is highly sensitive to the BH_2OH dissociation barrier. Increasing the BH_2OH dissociation barrier decreases the predicted rate of reaction; however, increasing or decreasing the activation barriers for other elementary steps by 5% does not affect the predicted rate of oxidation.

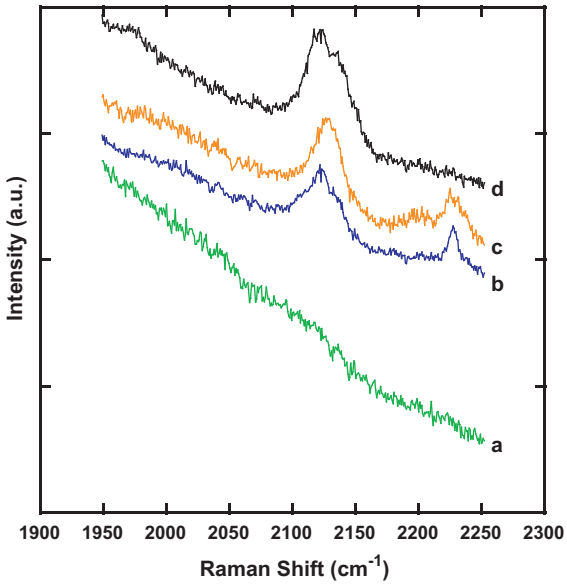

Fig. 11. Surface enhanced Raman spectra for borohydride oxidation over gold electrode at different potentials.

3.7. Surface enhanced Raman spectroscopy

Fig. 11 shows surface enhanced Raman spectra on a gold electrode following borohydride oxidation at various constant potentials held for 10 min. Two peaks are observed in the Raman spectra at approximately 2125 cm^{-1} and 2225 cm^{-1} after oxidation at −0.4 and −0.2 V, which are attributed to a stable intermediate adsorbate on the electrode surface. No peaks are observed associated with borohydride species at the lower potentials of −0.8 V. Because of the negligible barrier of B–O bond formation reactions, BH_2^*, $BHOH^*$ and $B(OH)_2^*$, are ruled out as possible stable surface intermediates. Four surface species, BH_4^*, BH_3^*, BH_2OH^* and $BH(OH)_2^*$, require B–H dissociation reactions for further conversion and are possible as stable intermediates. The vibrational frequencies of these surface species were calculated using DFT methods. The functional used in the DFT method (PW91) is known to systematically overestimate vibrational frequencies, and a scaling factor of 0.96 was used to correct the calculated frequencies [29].

Table 3
Corrected vibrational frequencies (cm^{-1}) in the B–H stretching range for possible stable intermediates over the Au(1 1 1) surface. A full list of vibrational frequencies of the adsorbed species is included in the supplementary information.

BH_4^*	BH_2OH^*	$BH(OH)_2^*$	BH_3^*
2335	2470	2461	2231
1932	2320		2204
1923			2124
1868			

The assignment of the observed Raman peaks to BH_4^*, BH_2OH^*, or $BH(OH)_2^*$ adsorbates can be ruled out by comparison with calculated frequencies. The corrected B–H bond stretching frequencies for BH_4^* species are 2335 cm^{-1}, 1932 cm^{-1}, 1923 cm^{-1} and 1868 cm^{-1} which do not closely match the observed frequencies in the Raman experiments. Due to the lower barrier of BH_4 dissociation on the surface, these species are not observed as stable intermediates in the SERS experiments. Similarly, the observed peaks in the SERS spectra could not correspond to BH_2OH or $BH(OH)_2$ species on the surface. Due to the very weak binding of these stable species on the Au(1 1 1) surface [5], any unreacted species of BH_2OH and $BH(OH)_2$ could desorb from the electrode surface upon removing the electrode from the reaction environment. Therefore, these species are not detected in the SERS experiments.

The corrected B–H vibrational frequency of BH_3 species on the Au(1 1 1) surface are 2231 cm^{-1}, 2204 cm^{-1} and 2124 cm^{-1} and reasonable agree with the experimentally observed spectra in Fig. 11. The substantial barrier of BH_3 dissociation and relatively stronger binding (−0.55 eV) of these species on the surface [5], allow detection of the BH_3^* intermediates as stable species on the surface. The observed Raman peaks could not be assigned to stable BH_3OH^* since corrected B–H vibrational frequencies for these species are all lower than 2000 cm^{-1}. The loss the higher frequency peak at −0.1 V and broadening of the lower frequency peak has not been explained, and may represent a change in coverage at higher oxidation rates.

All vibrational calculations considered intermediates at the metal–vacuum interface, and the presence of solvating water or surface electric fields may alter the absolute values of the vibrational frequencies. To quantify the vibrational shift induced due to hydrogen bonding with nearby water molecules, we calculated the vibration frequency of BH_3^* with 3 water molecules around the adsorbed borane species. The corrected vibration frequencies of B–H bonds at the desired region changed from 2231, 2204 and 2124 cm^{-1} to 2256, 2249 and 2163 cm^{-1}, respectively (see Table 3).

To the best of our knowledge there is only one in situ infrared study of the borohydride oxidation reaction over the gold electrode. Concha and coworkers reported a band at 1184 cm^{-1} which they assigned to a B–H bond of either BH_3 or BH_3OH^- species [30]. They also reported two other bands at 1326 and 1415 cm^{-1} which they assigned to the B–O bond of BO_2^- or BOB species. We did not considered B–O–B bond formation of BH_3OH^- species in our analysis.

4. Conclusions

A simple model was developed to calculate the potential dependent activation barriers of borohydride oxidation over the Au(1 1 1) surface. The kinetic region of the linear sweep voltammogram was simulated using density functional theory calculated reaction energetics and agrees with the experimental voltammogram. The predicted rate is sensitive to the electrochemical reaction symmetry factor and the BH_2OH dissociation barrier. A value of 0.44 is suggested for symmetry factor of borohydride oxidation reaction over the Au(1 1 1) surface. Both calculated and experimental kinetics are consistent with a single electron transfer limiting reaction step, which is determined to be associated with B–H bond dissociation of a surface intermediate.

Due to the substantial barrier of B–H dissociation, BH_3^*, BH_2OH^* and $BH(OH)_2^*$ are possible stable surface intermediates of the reaction, however, the LSV simulation suggests the surface is covered by a monolayer of BH_2OH^* at potentials higher than −0.55*V*(*NHE*). SERS was used to detect stable BH_3 intermediates on the electrode surface after oxidation at −0.2 and −0.4*V*(*NHE*). Comparison of SERS spectra, taken following removal of the electrode from the electrochemical cell, with DFT-calculated vibrational frequencies suggests a stable BH_3^* intermediate. The theory and experimental results are in qualitative agreement that stable intermediates are formed during borohydride oxidation containing B–H bonds, further suggesting the rate of borohydride electrooxidation is limited on Au electrodes by slow B–H dissociation.

Acknowledgement

This work was supported by the National Science Foundation, Grant # CBET-0730502.

Appendix A. List of variables

BE	binding energy of an adsorbate relative to the gas phase (eV, Eq. (2))
ΔG_1	Gibb's free energy change of adsorption of $BH_4^-{}_{aq}$ (eV, Eq. (3))
K_1	equilibrium constant for adsorption of the $BH_4^-{}_{aq}$ (unitless, Eq. (4))
T	temperature (K)
$[BH_4^-]$	dimensionless concentration of $BH_4^-{}_{aq}$ (unitless)
ΔG_2	Gibb's free energy change of adsorption of $OH^-{}_{aq}$ (eV, Eq. (6))
K_1	equilibrium constant for adsorption of the $OH^-{}_{aq}$ (unitless, Eq. (5))
$[OH^-]$	dimensionless concentration of $OH^-{}_{aq}$ (unitless)
ΔG_3	Gibb's free energy change of desorption of $B(OH)_3^*$ (eV, Eq. (8))
$[B(OH)_4^-]$	dimensionless concentration of $B(OH)_4^-{}_{aq}$ (unitless)
K_3	equilibrium constant for desorption of the $B(OH)_3^*$ (unitless, Eq. (9))
E_a	potential dependent activation barrier for an elementary reaction (eV, Eq. (13))
E_a°	activation barrier of an elementary step at the equilibrium potential for H* desorption (eV)
β	symmetry factor (unitless)
k_1	rate constant for dissociation of a B–H bond of BH_4^* (s^{-1} $site^{-1}$, Eq. (14))
A_1	pre-exponential factor within the rate constant for B–H dissociation of BH_4^* (s^{-1} $site^{-1}$)
r_n	rate of reaction n (s^{-1} $site^{-1}$, Eq. (16), reaction steps numbered in Fig. 1)
θ_n	fractional surface coverage of species n (unitless, species numbers in Fig. 1)
i_c	current in elementary units (electrons s^{-1} $site^{-1}$)
a	area occupied by 1 atom (cm^2)
A	surface area of experimental electrode (cm^2)
n	number of atoms per active site
N	total number of atoms on experimental electrode surface
S	total number of active sites on experimental electrode surface
I	current (A s^{-1})

Appendix B. Supplementary data

Supplementary data associated with this article can be found, in the online version, at doi:10.1016/j.jpowsour.2011.07.042.

References

[1] J.-H. Wee, J. Power Sources 161 (2006) 1–10.
[2] S. Suda, N. Morigasaki, Y. Iwase, Z.P. Li, J. Alloy Compd. 404-406 (2005) 643–647.
[3] C.P. de Leon, F.C. Walsh, D. Pletcher, D.J. Browning, J.B. Lakeman, J. Power Sources 155 (2006) 172–181.
[4] J.-H. Wee, J. Power Sources 155 (2006) 329–339.
[5] G. Rostamikia, M.J. Janik, J. Electrochem. Soc. 156 (2009) B86–B92.
[6] G. Rostamikia, M.J. Janik, Electrochim. Acta 55 (2010) 1175–1183.
[7] A.B. Anderson, T.V. Albu, Electrochem. Comm. 1 (1999) 203–206.
[8] C.D. Taylor, S.A. Wasileski, J.S. Filhol, M. Neurock, Phys. Rev. B 73 (2006) 165402.
[9] J.S. Filhol, M. Neurock, Angew. Chem. Int. Ed. 45 (2006) 402–406.
[10] S.A. Wasileski, M.J. Janik, Phys. Chem. Chem. Phys. 10 (2008) 3613–3627.
[11] M.J. Janik, C.D. Taylor, M. Neurock, J. Electrochem. Soc. 156 (2009) B126–B135.
[12] A.J. Bard, L.R. Faulkner, Electrochemical Methods: Fundamentals and Applications, John Wiley & Sons, Inc., 2001.
[13] E. Gyenge, Electrochim. Acta 49 (2004) 965–978.
[14] M.V. Mirkin, H. Yang, A.J. Bard, J. Electrochem. Soc. 139 (1992) 2212–2217.
[15] M. Chatenet, F. Micoud, I. Roche, E. Chainet, Electrochim. Acta 51 (2006) 5459–5467.
[16] M. Chatenet, F.H.B. Lima, E.A. Ticianelli, J. Electrochem. Soc. 157 (2010) B697–B704.
[17] D.A. Finkelstein, N.D. Mota, J.L. Cohen, H.D. Abruna, J. Phys. Chem. C 113 (2009) 19700–19712.
[18] Y.-C. Liu, K.-H. Yang, T.-C. Hsu, Anal. Chim. Acta 636 (2009) 13–18.
[19] Y.-C. Liu, C.-C. Yu, K.-H. Yang, J.-S. Chen, J. Electroanal. Chem. 611 (2007) 217–224.
[20] G. Kresse, J. Hafner, Phys. Rev. B 47 (1993) 558–561.
[21] G. Kresse, J. Furthmüller, Comput. Mater. Sci. 6 (1996) 15–50.
[22] G. Kresse, J. Furthmüller, Phys. Rev. B 54 (1996) 11169–11186.
[23] G. Kresse, D. Joubert, Phys. Rev. B 59 (1999) 1758.
[24] N.A.W. Holzwarth, G.E. Matthews, R.B. Dunning, A.R. Tackett, Y. Zeng, Phys. Rev. B 55 (1997) 2005.
[25] J.P. Perdew, J.A. Chevary, S.H. Vosko, K.A. Jackson, M.R. Pederson, D.J. Singh, C. Fiolhais, Phys. Rev. B 46 (1992) 6671–7895.
[26] G. Henkelman, B.P. Uberuaga, H. Jónsson, J. Chem. Phys. 113 (2000) 9901–9904.
[27] G. Henkelman, H. Jónsson, J. Chem. Phys. 113 (2000) 9978–9985.
[28] G. Prentice, Electrochemical Engineering Principles, Prentice Hall International Series, 1991.
[29] J.P. Merrick, D. Moran, L. Radom, J. Phys. Chem. A 111 (2007) 11683–11700.
[30] B.M. Concha, M. Chatenet, C. Coutanceau, F. Hahn, Electrochem. Comm. 11 (2009) 223–226.